BMC Neurology

RESEARCH

Open Access

Screening of signaling pathways and hub genes in Guillain-Barré syndrome based on bioinformatics and machine learning

Denger Zhang[1], Zhao Wang[2], Wei Ma[3] and Zhenhai Wang[4,5,6*]

Abstract

Background Guillain-Barré syndrome (GBS) is a acute immune-mediated peripheral neuropathy with scarce incidence, yet its molecular mechanisms remain incompletely elucidated. This study aims to systematically identify key hub genes and signaling pathways in GBS to uncover novel insights into its immunopathology and potential therapeutic targets.

Methods The transcriptomic dataset GSE31014, comprising peripheral blood leukocytes from 7 GBS patients and 7 healthy controls, was analyzed. Differentially expressed genes (DEGs) were identified using the Limma package. Functional enrichment was assessed via Gene Set Enrichment Analysis (GSEA). A protein-protein interaction (PPI) network was constructed to identify core modules, from which hub genes were pinpointed through the cross-validation of two machine learning algorithms: the Least Absolute Shrinkage and Selection Operator (LASSO) and Support Vector Machine-Recursive Feature Elimination (SVM-RFE). Immune cell infiltration was evaluated using single-sample GSEA (ssGSEA). Furthermore, upstream regulatory networks and potential therapeutic small molecules were predicted. The hub gene upregulation was validated by laboratory qRT-PCR and independent public datasets.

Results We identified 885 DEGs in GBS, which were significantly enriched in immune-related pathways such as chemokine signaling, B/T cell receptor signaling, and oxidative phosphorylation. PPI network and machine learning algorithms converged on two robust hub genes: HSP90AA1 and CAMP. Immune infiltration analysis revealed widespread activation of both innate and adaptive immune cells in GBS. HSP90AA1 expression correlated with B-cell and type 2 immune responses, while CAMP displayed a dual role, associated with both innate immune killing and the regulation of specific T-cell and NK-cell subsets. Both genes were co-enriched in the chemokine signaling pathway. FOXC1 was predicted as a common upstream transcriptional regulator. Additionally, five promising small-molecule therapeutics were screened. The significant upregulation of HSP90AA1 and CAMP in GBS was consistently validated.

Conclusion This integrated bioinformatics study identifies HSP90AA1 and CAMP as key hub genes in GBS, potentially driving neuroinflammation through the dysregulation of chemokine-mediated immune recruitment and activation. The findings offer novel insights into the immunopathogenesis of GBS and propose candidate molecules for future therapeutic development.

*Correspondence:
Zhenhai Wang
nyfywzh@163.com

Full list of author information is available at the end of the article

Keywords Guillain - Barré syndrome, Bioinformatics, Machine learning, HSP90AA1, CAMP, Immune infiltration

Introduction

GBS is an acute immune-mediated peripheral neuropathy characterized by demyelination and/or axonal injury of peripheral nerves [1]. It develops in genetically susceptible individuals following exposure to specific environmental triggers, such as infections with Campylobacter jejuni or cytomegalovirus, which initiate an abnormal immune response against the nervous system through molecular mimicry [2–4]. Intravenous immunoglobulin and plasma exchange are first-line immunomodulatory therapies commonly used in clinical practice; however, many patients experience inadequate treatment responses, incomplete functional recovery, or persistent neurological deficits, highlighting the limitations of current immunomodulatory strategies [5]. Additionally, GBS has a low incidence rate, making it challenging to obtain large-scale clinical datasets. This hinders a comprehensive understanding of its pathogenesis. Therefore, systematically exploring the molecular mechanisms of GBS is clinically significant for developing more targeted diagnostic tools and therapeutic interventions.

Previous research on GBS has primarily concentrated on humoral biomarkers, including anti-ganglioside antibodies, neurofilament proteins, and cytokines found in serum or cerebrospinal fluid [6–12]. Although these studies have partially illuminated the immunoinflammatory aspects of GBS, they have been confined to narrow downstream pathological events, neglecting to systematically explore the regulatory networks. This approach has clear limitations when addressing GBS as a complex neuroimmune disorder, with synergistic or cascading interactions among multiple genes and signaling pathways throughout the disease progression.Such methodological constraints also impede clinical translation. For example, while anti-ganglioside antibodies are helpful for subtyping, they do not consistently correlate with disease severity or treatment response [13, 14]. Similarly, targeted therapies such as eculizumab, a monoclonal antibody against complement C5, failed to significantly improve motor recovery in severe GBS during a phase III trial [15]. Additionally, in two randomized, double-blind, placebo-controlled phase II trials, eculizumab did not demonstrate a significant benefit in disability levels at 4 weeks compared to immunoglobulin alone [1]. These results imply that GBS pathogenesis does not stem from a single linear pathway but rather arises from dysregulation within complex molecular networks. The neglect of systemic mechanisms not only restricts etiological understanding but also constrains current treatments,, lacking precision targeting of key pathogenic nodes.

Omic approaches, which are based on high-throughput data, have been established for the comprehensive understanding of complex diseases [10].However, conventional differential expression analysis failed to distinguish pivotal regulators from background noise. This approach is also susceptible to gene collinearity, which may compromise the reliability of findings [16, 17]. Within this context, machine learning algorithms offer distinct advantages. LASSO regression, which employs L1 regularization, is adept at handling high-dimensional data, effectively mitigating variable collinearity while enabling precise identification of key determinants. SVM-RFE uses iterative optimization to robustly select the most discriminative gene combinations from complex feature sets. Integrating these algorithms into GBS research is expected to enhance the accuracy and reliability of hub gene identification, thereby providing new perspectives for elucidating the immunoregulatory mechanisms in GBS.

Therefore, we applied an integrated bioinformatics and machine learning algorithm to systematically identify core pathways and hub genes within the peripheral immune microenvironment of GBS. Utilizing the GSE31014 transcriptomic dataset from peripheral blood leukocytes, we conducted differential expression analysis, gene set enrichment analysis, and constructed a PPI network. Comparing to its original research [18], our study employs a unique, integrative computational strategy with several key advancements.Therefore, the LASSO and SVM-RFE were applied to identify more robust central hub genes based on their discriminative power and network centrality, rather than relying solely on fold-change magnitude. Furthermore, Immune cell infiltration and single-gene GSEA analysis were used to conduct a comprehensive characterization of the peripheral immune cell infiltration landscape and its correlation with these hub genes. Finally, multilevel validation was performed using independent clinical samples and public datasets to systematically decipher the molecular mechanisms of peripheral immune dysregulation in GBS(Overall flowchart, Fig. 1). These approaches enables us to extract novel systemic insights from this valuable public resource.

Materials and methods

Discovery set source

Gene expression profiles were extracted from the Gene Expression Omnibus (GEO) database (http://www.ncbi.nlm.nih.gov/geo) using "Guillain-Barré syndrome" as search criteria. The dataset GSE31014, derived from "Homo sapiens" samples, along with the platform GPL96,

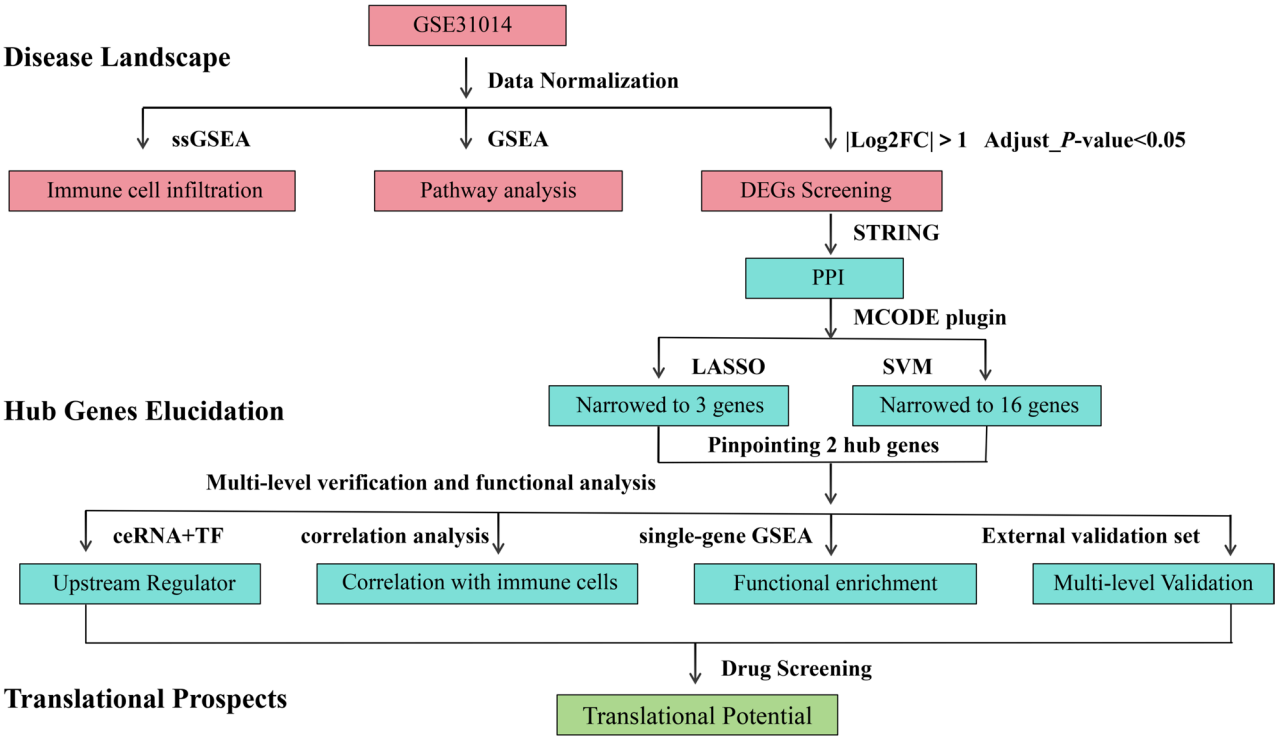

Fig. 1 Overall workflow of the integrated bioinformatics and machine learning analysis for identifying hub genes in GBS. The flowchart delineates the stepwise analytical pipeline employed in this study: I. Disease Landscape: The peripheral blood leukocyte transcriptomic dataset GSE31014 (7 GBS patients vs. 7 healthy controls) was acquired from the GEO database. After data normalization and quality control, differential expression analysis identified DEGs. Functional implications of the DEGs were explored through GSEA for pathways and ssGSEA for immune cell infiltration profiling. II. Hub Genes Elucidation: A PPI network was constructed from the DEGs, and its most interconnected region (Core Module I) was extracted. To pinpoint central regulators, two machine learning algorithms, LASSO and SVM-RFE, were applied to genes within this module for cross-validated feature selection, converging on two hub genes (HSP90AA1 and CAMP). Their biological roles were then investigated via correlation analysis with immune cells, single-gene GSEA for pathway association, and construction of a ceRNA and TF network to identify upstream regulators (e.g., FOXC1).The upregulation of the identified hub genes were rigorously validated across multiple levels: via qRT-PCR in an independent clinical cohort, in a separate human whole-blood transcriptomic dataset (GSE211225), and in a cross-species animal model dataset (GSE133750, EAN in rats). III. Translational Prospects: The translational potential was assessed by screening for potential therapeutic small molecules targeting Core Module I genes

was selected for analysis. It encompasses peripheral blood leukocyte samples from seven GBS patients and seven healthy controls.The selection of GSE31014 as the sole discovery cohort was based on considerations of methodological consistency. This dataset provides purified peripheral blood leukocyte samples (the target immune population) and uses a uniform microarray platform (GPL96), which can minimize the impact of sample heterogeneity and technical batch effects on the initial analysis to the greatest extent.

Screening of DEGs

Differentially expressed genes (DEGs) were identified from the GSE31014 dataset using the Limma package in R. The raw microarray data were preprocessed and normalized to eliminate non-biological technical variations. Probes were first annotated to genes based on the platform annotation file. For genes mapped by multiple probes, expression values were consolidated by averaging, while probes matching multiple genes or no genes were excluded. Subsequently, normalization was performed across all arrays using the normalizeBetweenArrays method. Consistent with recent transcriptome studies [19, 20], we applied the conventional and stringent cutoff of $|\log2FC| > 1$ and an adjusted P-value < 0.05 (using the Benjamini-Hochberg false discovery rate (FDR) method) to prioritize genes exhibiting substantial expression changes, thereby enhancing the reliability of all downstream analyses. Visualization of the results was achieved by generating a gene heatmap and a volcano plot using the ComplexHeatmap and ggplot2 packages, respectively.

GSEA

GSEA was utilized to identify potential signaling pathways and biological processes involved in the pathogenesis of GBS. GSEA is a computational method that determines whether a predefined set of genes exhibits statistically significant, concordant differences between two biological states. The analysis was conducted using

the GSEA software with default parameters, including the weighted enrichment statistic method. Reference gene sets were obtained from the GSEA-MSigDB database, specifically the c2.cp.kegg_legacy.v2025.1.Hs.symbols.gmt (KEGG canonical pathways) and c5.go.bp.v2025.1.Hs.symbols.gmt (Gene Ontology biological processes) collections. Gene sets with absolute normalized enrichment score (NES) values > 1, false discovery rate (FDR) q-values < 0.25, and adjusted *P*-values < 0.05 were considered statistically significant.

Analysis of the core modules of DEGs

DEGs were incorporated into the STRING database (https://string-db.org/) to facilitate PPI analysis. Subsequently, the data were integrated into Cytoscape version 3.9.0 using a .txt file.The core module (designated as Core Module I) was identified using the following default parameters: Degree Cutoff = 2, Node Score Cutoff = 0.2, K-Core = 2, and Max. Depth = 100. To evaluate the robustness of the identified Core Module I, a sensitivity analysis was performed by varying the network stringency parameters (testing Degree Cutoff = 3, K-Core = 3 and Degree Cutoff = 4, K-Core = 4).

Hub genetic analysis

The LASSO method enhances linear regression by incorporating a penalty term—lambda times the absolute slope value—to mitigate model overfitting and bolster its predictive robustness. In contrast, the SVM is an established supervised learning approach, prevalently applied in classification and regression tasks, to select superior genes through the RFE technique. Consequently, this research employed SVM-RFE in conjunction with LASSO for the efficacious selection of highly discriminative genes within the principal core module I of the PPI network. The intersecting set from both LASSO and SVM-RFE served to designate the hub genes.

Assessment of immune cell infiltration by ssGSEA

To evaluate the relative infiltration levels of immune cells in the samples, we utilized the ssGSEA algorithm. The analysis was conducted using the GSVA package in R software, which transforms gene expression profiles into gene set enrichment scores. The immune cell gene signatures used for ssGSEA were derived from the authoritative study by Bindea et al. [21], which defines a curated set of marker genes for 28 distinct immune cell types. These have been extensively validated and are widely used for deconvoluting immune cell landscapes across diverse neuroinflammatory disorders [22, 23]. The ssGSEA algorithm converts the gene expression profile of each immune cell type into an enrichment score, representing the relative abundance of that specific cell type within an individual sample. This process yielded a matrix containing enrichment scores for all immune cells across every sample. Differences in immune cell infiltration levels between the control and GBS groups were subsequently assessed using the Wilcoxon rank-sum test for two-group comparisons.

Analysis of immune cell co-regulation network

To investigate the coordination among different immune populations in GBS, we analyzed the correlations between the enrichment scores of all immune cell types using Spearman's rank correlation. The resulting correlation matrix was visualized as a heatmap using the ggplot2 package.

Association between hub genes and immune phenotypes

To explore the potential immunomodulatory roles of the identified hub genes, we integrated the expression matrices of HSP90AA1 and CAMP with the immune cell enrichment scores. Spearman's correlation analysis was then employed to assess the relationships between hub gene expression and immune cell infiltration levels.

GSEA for hub genes

Reference gene sets were downloaded from the GSEA-MSigDB database (c2.cp.kegg_legacy.v2025.1.Hs.symbols.gmt). To investigate the potential roles of HSP90AA1 and CAMP in GBS pathogenesis, GBS samples were stratified into high- and low-expression groups based on the median expression levels of each gene. Genome-wide expression profiles of these subgroups were then subjected to GSEA using the default weighted enrichment statistic method. Significantly enriched pathways were identified using the following thresholds: an absolute normalized enrichment score (NES) > 1, a false discovery rate (FDR) q-value < 0.25, and an adjusted *P*-value < 0.05.

Transcription factors for hub genes and network construction of ceRNA

NetworkAnalyst functions as a comprehensive online platform for exploring biological interpretations, functions, and mechanisms via gene expression data analysis. In this research, NetworkAnalyst was utilized to investigate transcription factors associated with hub genes. Moreover, predictions of miRNAs for hub genes were cross-referenced using the Starbase(a comprehensive platform integrating CLIP-seq high-throughput experimental data and computational predictions), miRTarBase (a curated collection of experimentally validated miRNA–mRNA interactions), and TargetScan databases(a leading database for predicting miRNA–mRNA targeting relationships), with only miRNAs unanimously recognized by all three databases retained to enhance predictive accuracy. Additionally, the spongeScan database was used to facilitate LncRNA predictions

for miRNAs identified by these databases, aiding in the construction of the ceRNA network. The integrated lncRNA-miRNA-mRNA-TF interaction network was ultimately assembled and visualized using Cytoscape software (version 3.9.2).

Small-molecule screening of genes in the core modules

Enrichr stands as a widely recognized portal, offering an expansive, varied library of gene sets for genome-wide enrichment exploration. The Drug Signatures Database (DSigDB) acts as a comprehensive repository, housing 22,527 gene sets, and serves to identify drug candidates targeting DEGs. Access to DSigDB is facilitated via the Diseases/Drugs section within Enrichr. Consequently, this research harnessed DSigDB via Enrichr to pinpoint potential therapeutic small molecules corresponding to genes within the core module I .

Clinical samples collection

Peripheral blood samples were collected from 3 GBS patients and 3 healthy controls at the General Hospital of Ningxia Medical University. The inclusion criteria for GBS patients were based on the "European Academy of Neurology/Peripheral Nerve Society Guideline on diagnosis and treatment of Guillain-Barré syndrome" [24]. Exclusion criteria included: (1) active systemic infections; (2) comorbid autoimmune disorders; (3) history of malignancies; (4) chronic hepatic, renal, or cardiac insufficiency. All participants provided written informed consent before sample collection. The study protocol was approved by the Medical Research Ethics Review Committee of General Hospital of Ningxia Medical University (Ethical number: 2018 – 318).

Isolation of human peripheral blood leukocytes

Human peripheral blood leukocytes were isolated using Red Blood Cell (RBC) Lysis Buffer (Solarbio, China). One volume of fresh whole blood was mixed with three volumes of RBC lysis buffer. The mixture was incubated on ice for 15 min, with gentle vortexing twice during this period. Subsequently, the sample was centrifuged at 450 × g for 10 min at 4 °C to pellet the leukocytes, and the supernatant was carefully aspirated. The leukocyte pellet was resuspended in two volumes of RBC lysis buffer by gentle vortexing and centrifuged again under the same conditions (450 × g, 10 min, 4 °C). After complete removal of the supernatant, the purified leukocytes were resuspended in an appropriate buffer for subsequent qRT-PCR analysis.

qRT-PCR validation of HSP90AA1 and CAMP expression in human peripheral blood leukocytes

Total RNA was extracted from human peripheral blood leukocytes using the RNA simple-Total RNA isolation kit (Tiangen, China). Total RNA was reverse-transcribed into cDNA using the PrimeScript RT reagent kit (TaKaRa, Japan), and then the cDNA was used for RT-qPCR with TB Green Premix Ex Taq Ⅱ (Tli RNaseH Plus) (TaKaRa, Japan). The relative expression of mRNA was normalized to GAPDH using the comparative CT method (ΔΔCT). Primer sequencesused used for qRT-PCR validation are listed in Supplementary Table 1.

Validation set source

To independently validate our findings, we obtained two distinct transcriptomic datasets from the GEO database (http://www.ncbi.nlm.nih.gov/geo). The GSE211225 datas et was selected as our primary human validation cohort. It comprises whole-blood mRNA samples from 6 patients in the acute phase of GBS, 10 patients in the post-acute phase, and 6 healthy controls, profiled by RNA sequencing (RNA-seq). We chose this dataset for validation for two key reasons: first, it represents an independent cohort; second, its use of RNA-seq technology allows us to test whether the hub genes identified from our microarray-based discovery cohort (GSE31014) are robust across different profiling platforms, thereby assessing the generalizability of our findings. The GSE133750 dataset was selected for cross-species validation. It provides transcriptomic data from sciatic nerve tissues of Lewis rats with experimental autoimmune neuritis (EAN), a well-established model that recapitulates key pathological features of human GBS. The original study profiled sciatic nerves from 8–10-week-old Lewis rats across disease timepoints: control, early neuritis (10 days post-induction), peak neuritis (19 days), and late neuritis (30 days), with $n = 3$ biological replicates per group. We utilized these two datasets for independent validation, which allowed us to more rigorously demonstrate the universality of the identified hub genes across various technologies, sample types, and even species.

Statistical analysis

All statistical analyses and graphical representations were performed using R software and GraphPad Prism 8.0 (GraphPad Software Inc.). Measurement data conforming to a normal distribution are expressed as the mean ± standard deviation($\bar{x} \pm s$), and intergroup comparisons were conducted using independent-sample t-tests. Non-normally distributed data are expressed as the median (interquartile range) [M (IQR)], and the Mann-Whitney U test was used for intergroup comparisons. Categorical data are presented as constituent ratios or rates and were analyzed using the chi-square test or Fisher's exact test, as appropriate. Spearman's rank correlation analysis was employed to explore the correlations between hub gene expression and immune infiltration levels. The diagnostic efficacy of the two hub genes was

evaluated using receiver operating characteristic (ROC) curve analysis, with results expressed as the area under the curve (AUC) and its 95% confidence interval (CI). The sensitivity, specificity, positive predictive value (PPV), and negative predictive value (NPV) for each gene were calculated, with the optimal cut-off value determined by maximizing the Youden index. In figures, significance levels are denoted as follows: $^{*}P<0.05$, $^{**}P<0.01$, and $^{***}P<0.001$.

Results

Transcriptomic profiling of peripheral blood leukocytes reveals immune and metabolic dysregulation in GBS

To comprehensively characterize the peripheral immune molecular features of GBS, we began our analysis with quality control and a global assessment of the GSE31014 dataset from the GEO database. This dataset comprises global gene expression microarray data from peripheral blood leukocytes of 7 GBS patients and 7 healthy controls. After excluding two outlier samples from the control group, principal component analysis (PCA) revealed a clear segregation between the GBS and control groups (Fig. 2A), supporting the presence of systematic transcriptomic differences. Differential gene expression analysis was conducted using the Limma package, identifying a total of 885 DEGs under the thresholds of absolute Log2FC > 1 and adjusted *P*-value < 0.05. Among these, 776 genes were significantly upregulated and 109 were significantly downregulated. The volcano plot and heatmap visually represent these findings(Fig. 2B-C).

To elucidate the biological implications of the identified DEGs, we performed GSEA. The enrichment outcomes were visualized with "ggplot2," adhering to screening parameters of absolute NES values > 1, FDR < 0.25, and adjusted *P*-value < 0.05. GSEA-KEGG revealed significant enrichment of GBS-associated genes in several key pathways, including B-cell receptor signaling(NES = 2.107, $P<0.001$)(Fig. 3A), Fc gamma R-mediated phagocytosis(NES = 2.081, $P<0.001$)(Fig. 3B), Toll-like receptor signaling(NES = 2.075, $P<0.001$)(Fig. 3C), chemokine signaling(NES = 1.852, $P<0.001$)(Fig. 3D), NOD-like receptor signaling pathway(NES = 2.009, $P<0.001$)(Fig. 3E), T-cell receptor signaling(NES = 1.755, $P<0.01$)(Fig. 3F), leukocyte transendothelial migration (NES = 1.655, $P<0.01$)(Fig. 3G), natural killer cell-mediated cytotoxicity(NES = 1.588, $P<0.05$)(Fig. 3H) and Oxidative Phosphorylation(NES = 2.052, $P<0.001$) (Fig. 3I). In parallel, GSEA-GO biological process analysis highlighted enrichment in processes such as regulation of innate immune response(NES = 2.370, $P<0.001$), leukocyte mediated immunity(NES = 1.923, $P<0.001$),T cell activation(NES = 1.772, $P<0.001$), and B cell activation(NES = 1.840, $P<0.001$)(Fig. 3J) Together, these results suggest that the peripheral immune system in GBS patients undergoes broad activation and dysregulation, coupled with marked metabolic disorder.

Pinpointing GBS key hub genes involved in immune dysregulation through integrated machine learning algorithms

To identify functionally cohesive units within the complex interactome, we constructed a PPI network from all DEGs using the STRING database and subsequently performed cluster analysis with the MCODE plugin in Cytoscape. This approach successfully identified a highly interconnected subnetwork, designated as Core Module I, which comprises 69 nodes and 399 edges (Fig. 4A). Screening parameters for MCODE were set as follows: Degree Cutoff = 2, Node Score Cutoff = 0.2, K-Core = 2, and Max Depth = 100. This standard has been adopted in numerous bioinformatics studies [25, 26].To evaluate the robustness of the identified Core Module I, we performed a sensitivity analysis by varying the network stringency parameters (testing Degree Cutoff = 3, K-Core = 3 and Degree Cutoff = 4, K-Core = 4). Reassuringly, both hub genes, HSP90AA1 and CAMP, were consistently retained within the primary core module under these more stringent conditions (Supplementary Fig. 1). This result underscores the stability of our module identification and reinforces that Core Module I, as the densely connected region in the PPI network, represents a robust and functionally cohesive unit, making it an ideal candidate pool for subsequent hub gene screening.

To pinpoint the most central genes from Core Module I, we employed two complementary machine learning algorithms for cross-validation. The LASSO regression model, advantageous for handling multicollinearity, narrowed the candidate genes to HSP90AA1, BCL6, and CAMP (Fig. 4B). Concurrently, the SVM-RFE algorithm selected a feature set comprising 16 genes, including CASP1, CAMP, CBX3, CCR2, EIF3H, TLR8, LY96, ATP5J, DOCK2, RAF1, BCL2L1, TBK1, SF3B1, HSP90AA1, SNW1, and MYC (Fig. 4C). The intersection of results from both methods conclusively identified HSP90AA1 and CAMP as the consensus hub genes (Fig. 4D). This multi-algorithm consensus strategy significantly strengthens the reliability of HSP90AA1 and CAMP as key hub genes in GBS.

We further assessed the ability of HSP90AA1 and CAMP to distinguish GBS patients from healthy individuals. ROC curve analysis performed on the training dataset (GSE31014) demonstrated diagnostic potential for both genes. Specifically, HSP90AA1 achieved an AUC of [0.714 (95% CI: 0.353–1.000)](Fig. 4E), while CAMP yielded an AUC of [0.939 (95% CI: 0.806–1.000)](Fig. 4F). Specific values are provided in Supplementary Table 2. Thus, through a process spanning from network-based discovery to diagnostic validation, HSP90AA1 and

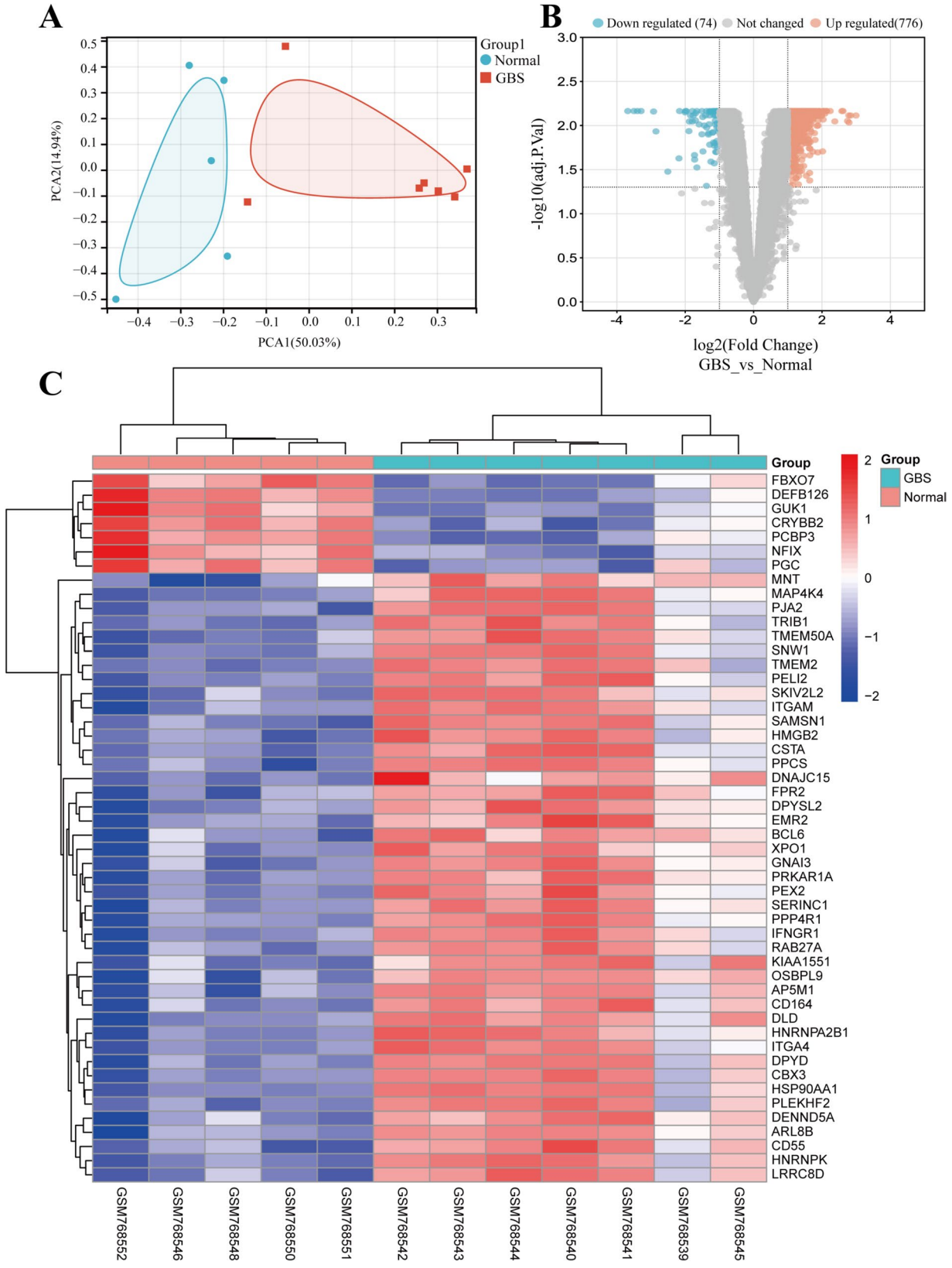

Fig. 2 Visualization of differentially expressed genes. **A** Principal component analysis (PCA) of the GSE31014 dataset, demonstrating distinct clustering between GBS patients ($n=7$) and healthy controls ($n=5$). **B** Volcano plot of differentially expressed genes (DEGs) identified by the Limma package (|log-2FC|≥1, adjusted *P*-value < 0.05), highlighting 776 upregulated (orange) and 109 downregulated (blue) genes. **C** Heatmap of the top 50 DEGs, illustrating hierarchical clustering of samples and gene expression patterns

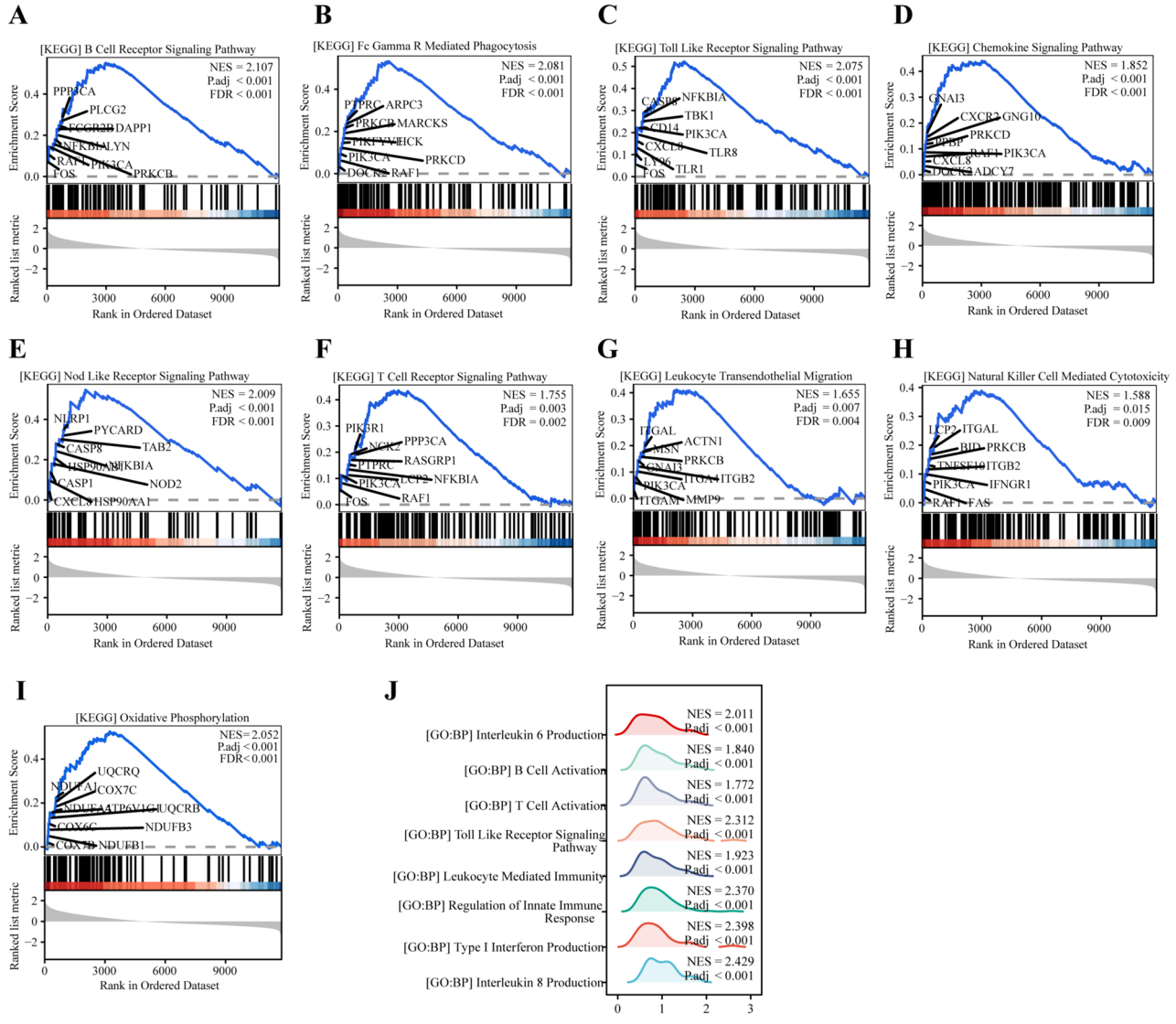

Fig. 3 GSEA reveals activated immune and metabolic pathways in GBS. **A**-**I** GSEA - KEGG analysis reveals significant enrichment of the B - cell receptor signaling pathway, Fc gamma R - mediated phagocytosis, Toll - like receptor signaling pathway, chemokine signaling pathway, NOD - like receptor signaling pathway, T - cell receptor signaling pathway, leukocyte transendothelial migration, natural killer cell - mediated cytotoxicity, and Oxidative Phosphorylation. **J** GSEA-GO biological process analysis enrichments include interleukin-8 production, type I interferon production, regulation of the innate immune response, leukocyte-mediated immunity, toll-like receptor signaling pathway, T cell activation, B cell activation, and interleukin-6 production

CAMP were systematically established as reliable and promising candidates central to GBS pathology.

Hub genes HSP90AA1 and CAMP orchestrate distinct immune activation pathways in GBS

To elucidate the role of hub genes in remodeling the immune microenvironment of GBS, we systematically evaluated the activity of 28 immune cell subsets using ssGSEA. Comparative analysis revealed significantly elevated ssGSEA scores in GBS patients compared to healthy controls across multiple immune cell populations, including activated B cells, activated CD4⁺ T cells, activated CD8⁺ T cells, central memory CD4⁺ T cells, effector memory CD8⁺ T cells, gamma delta T cells, immature B cells, type 2 T helper cells, immature dendritic cells, macrophages, mast cells, myeloid-derived suppressor cells (MDSCs), natural killer T cells, neutrophils, and plasmacytoid dendritic cells (Fig. 5A)(all $P < 0.05$). These findings indicate widespread activation of the peripheral immune system during the pathogenesis of GBS, involving the coordinated participation of both adaptive and innate immune compartments. Specific values are provided in Supplementary Table 3.

Further analysis demonstrated significant positive correlations among these immune cell subsets, forming a coordinated co-activation network (Fig. 5B). This suggests that the immune response in GBS represents a synchronized, system-wide process rather than isolated

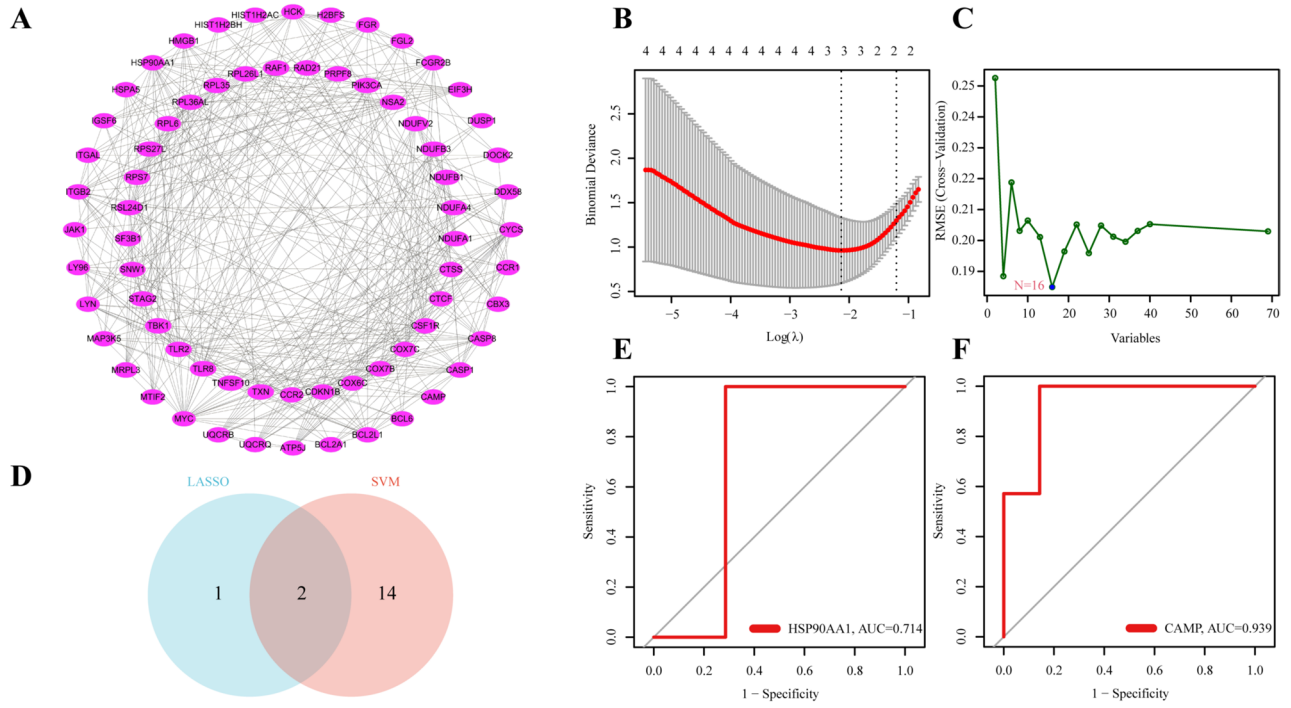

Fig. 4 Pinpointing GBS hub genes. **A** Analysis of the core module I in the protein interaction network of differentially expressed genes.The PPI network was constructed using the STRING database for 885 DEGs. The core module I consists of 69 nodes and 399 edges, identified using the MCODE plugin in Cytoscape (with the following parameters: Degree Cutoff = 2, Node Score Cutoff = 0.2, K-Core = 2, Max Depth = 100). **B**-**C** Hub gene screening by LASSO and SVM algorithm. LASSO regression analysis of core module I genes, selecting HSP90AA1, BCL6, and CAMP as key candidates.SVM-RFE algorithm identifying 16 hub genes. **D** Intersection gene analysis of the two algorithms.Venn diagram showing overlap between LASSO and SVM-RFE results, with HSP90AA1 and CAMP as consensus hub genes. **E**-**F** ROC curves for HSP90AA1 and CAMP were analyzed, with HSP90AA1 achieving an AUC of 0.714 (95% CI: 0.353–1.000), and CAMP resulting in an AUC of 0.939 (95% CI: 0.806–1.000)

cellular events. To identify potential upstream drivers of this coordinated immune phenotype, we investigated the specific roles of the hub genes HSP90AA1 and CAMP.

Correlation analysis revealed distinct immunomodulatory patterns for each hub gene (Fig. 5C). HSP90AA1 expression exhibited significant positive correlations with B cell and type 2 immune responses, including activated B cells ($R = 0.86$), effector memory CD8⁺ T cells ($R = 0.82$), type 2 T helper cells ($R = 0.75$), and plasmacytoid dendritic cells ($R = 0.75$). Single-gene GSEA for HSP90AA1(Fig. 5D) further confirmed its significant enrichment in the B cell receptor signaling pathway (NES = 2.255, $P < 0.001$) and T cell receptor signaling pathway (NES = 1.727, $P < 0.01$), offering mechanistic insights into its broad association with adaptive immune cells. Concurrently, its positive correlations with innate immune cells, such as gamma delta T cells ($R = 0.68$), aligned with significant enrichment in the chemokine signaling pathway (NES = 2.097, $P < 0.001$), suggesting HSP90AA1 may coordinate widespread immune cell recruitment through this mechanism. In contrast, CAMP presented a more complex and dual immunomodulatory profile. It demonstrated a significant positive correlation with T follicular helper (Tfh) cells ($R = 0.61$), a key CD4⁺ T cell subset for B-cell help.Concurrently, it exhibited significant negative correlations with activated CD4⁺ T cells (R = -0.68) and immunoregulatory CD56bright natural killer cells (R = -0.71). This suggests that CAMP may simultaneously promote certain humoral immune axes while suppressing other cellular and regulatory immune compartments. Single-gene GSEA for CAMP provided further mechanistic insights(Fig. 5E). The positive correlation of CAMP with CD56dim natural killer cells ($R = 0.61$) was supported by its significant enrichment in natural killer cell-mediated cytotoxicity (NES = 1.992, $P < 0.001$) and Fc gamma R-mediated phagocytosis (NES = 1.793, $P < 0.05$), underscoring its role in innate immune killing. Additionally, its enrichment in the chemokine signaling pathway (NES = 1.654, $P < 0.01$) and leukocyte transendothelial migration (NES = 1.680, $P < 0.05$) points to a potential role in directing immune cell trafficking and tissue infiltration in GBS. Notably, the chemokine signaling pathway was commonly enriched for both hub genes, indicating that HSP90AA1 and CAMP may collaborate to regulate the directional migration and tissue infiltration of immune cells, thus playing a critical role in the neuroinflammatory process of GBS.

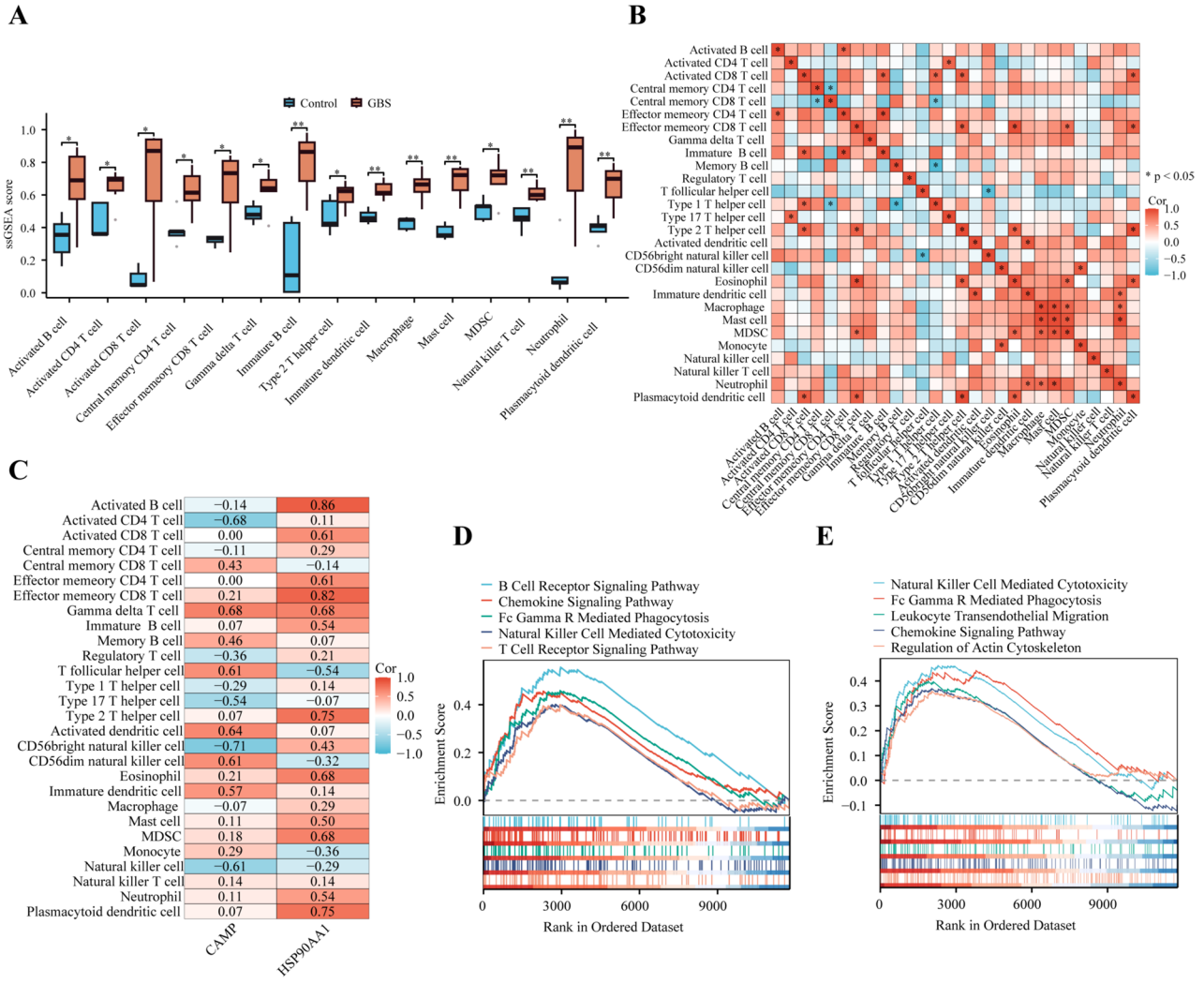

Fig. 5 Hub genes HSP90AA1 and CAMP orchestrate distinct Immune Activation pathways in GBS. **A** Comparison of immune cell infiltration levels between GBS patients and healthy controls, as assessed by ssGSEA. **B** Correlation matrix depicting the interrelationships among various immune cell subsets in GBS. Red indicates positive correlations, and blue indicates negative correlations. **C** Correlation analysis between hub gene expression (HSP90AA1 and CAMP) and immune cell infiltration scores. **D** Single-gene GSEA reveals the signaling pathways associated with high expression of HSP90AA1. **E** Single-gene GSEA reveals the signaling pathways associated with high expression of CAMP

FOXC1 is a common upstream regulator of hub genes in a ceRNA-transcription factor network

To elucidate the upstream regulatory mechanisms controlling HSP90AA1 and CAMP expression, we constructed a comprehensive competing endogenous RNA (ceRNA) network through integrated bioinformatics analysis. miRNA predictions were obtained by cross-referencing three established databases (Starbase, miRTarBase, and TargetScan), retaining only miRNAs consistently identified across all platforms to ensure prediction reliability. This stringent approach identified 7 key miRNAs (hsa-miR-362-5p, hsa-miR-889-3p, hsa-miR-656-3p, hsa-miR-185-5p, hsa-miR-374a-3p, hsa-miR-186-5p, and hsa-miR-139-5p). Subsequently, lncRNA predictions for these miRNAs were generated using the spongeScan database, revealing 7 candidate lncRNAs (RP11-526P6.1, LINC00240, RP11-429B14.4, CTC-265F19.1, PKD1P6, RP11-99L13.2, and AC015849.16). Furthermore, transcription factor analysis using NetworkAnalyst identified FOXC1 as a common predicted regulator for both HSP90AA1 and CAMP (Fig. 6).This multi-layered regulatory network, comprising lncRNAs, miRNAs, and transcription factors, provides novel insights into the upstream control of GBS-associated gene expression and suggests complex post-transcriptional and transcriptional coordination in GBS pathogenesis.

Screening of potential therapeutic small molecules based on the core gene module I

To explore the translational potential of our findings, we screened the DSigDB database to identify potential

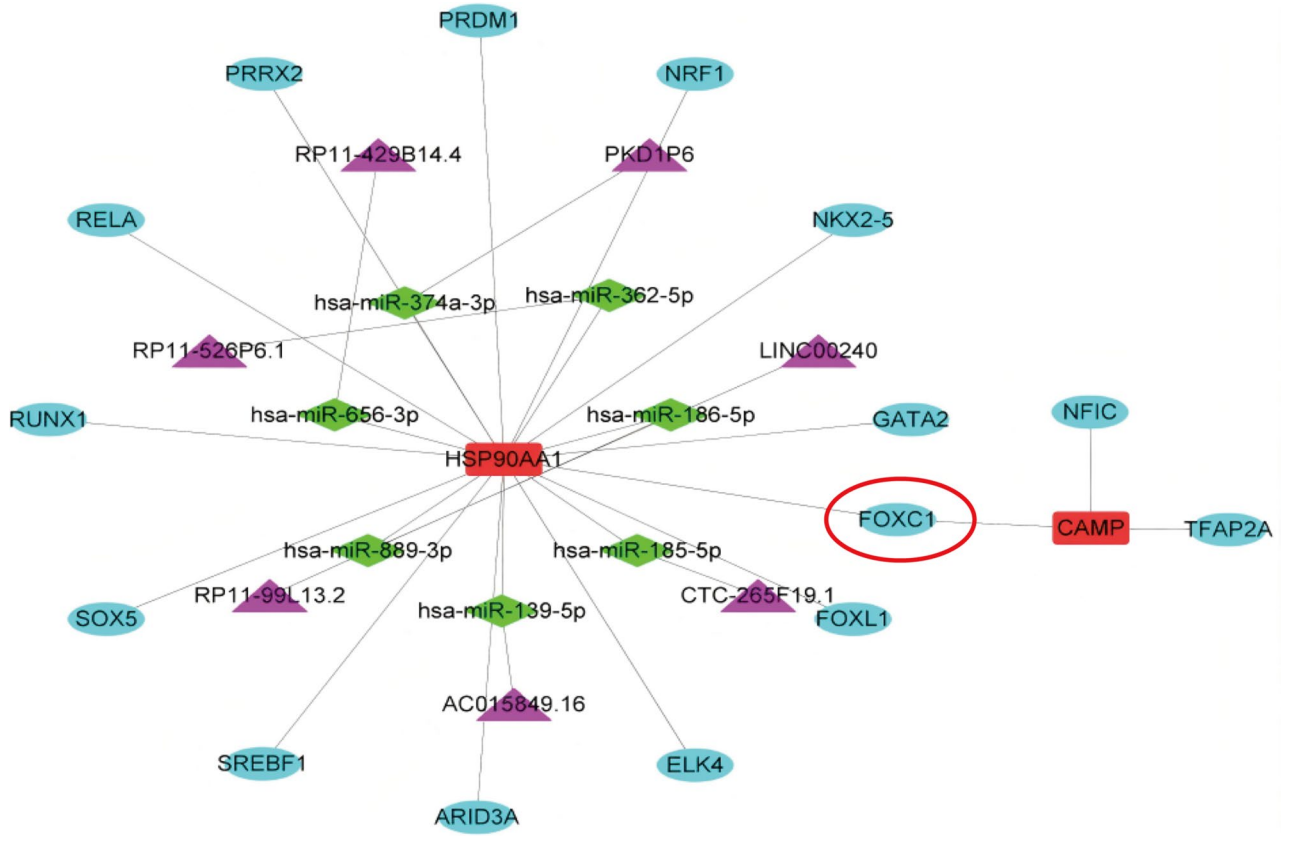

Fig. 6 Predict the upstream regulator of hub genes in a ceRNA-Transcription Factor Network. The network integrates predictions from multiple databases: miRNAs targeting hub genes were identified by intersecting Starbase, miRTarBase, and TargetScan; lncRNAs interacting with these miRNAs were predicted using SpongeScan; and transcription factors (TFs) were analyzed via NetworkAnalyst. FOXC1 was identified as a common transcription factor regulating both hub genes

therapeutic compounds targeting genes in Core Module I. The top eight candidate small molecules, ranked by Adjust_*P*-value. To enhance clinical relevance, we conducted a literature retrieval. Three compounds—arsenous acid (known neurotoxicity), bortezomib (associated with peripheral neuropathy) [27, 28], and danthron (lacking neuro-mechanistic studies)—were excluded due to safety or mechanistic concerns.The five remaining candidates are listed in Table 1.

We classified the remaining five compounds with more definite anti-inflammatory, immunomodulatory or antioxidant effects as potential candidate drugs. Literature searches revealed that some of the known mechanisms of these drugs are associated with the other findings of this study. For instance, simvastatin was reported to inhibit the secretion of CCL2 induced by TNF-α, thereby affecting the recruitment of leukocyte [29], which is related to the chemokine signaling pathway enriched in this study. Additionally, simvastatin [30]and N-acetylcysteine (NAC) [31]have both been confirmed to have immunomodulatory or anti-inflammatory properties. It is notable that some studies suggest that simvastatin [32] and sorafenib [33]may affect the function of HSP90 either directly or indirectly. Resveratrol also shows anti-inflammatory effects in neural inflammation models [34]. Specifically, simvastatin has been proven to directly upregulate the expression of the CAMP gene in epithelial cells, without relying on its lipid-lowering pathway, thereby enhancing the antibacterial defense [35].

Collectively, these computational predictions, coupled with established mechanistic evidence, nominate these five compounds as promising candidates worthy of further investigation as potential therapeutic strategies for GBS.

Laboratory qRT-PCR and independent public datasets validate hub gene upregulation in GBS across species

Based on the analysis of the GSE31014 dataset, both HSP90AA1 ($P<0.01$) (Fig. 7A) and CAMP ($P<0.01$) (Fig. 7B)were found to be significantly upregulated in the GBS group compared to healthy controls. To further validate the reproducibility and clinical relevance of our findings, we performed qRT-PCR analysis on peripheral blood leukocytes from 3 acute-phase GBS patients and 3 matched healthy controls. The groups were well-matched in baseline characteristics, including age and

Table 1 Potential drug molecules for genes in core module 1

Name	Adjust_*P*	Chemical Formula	Structure
FENRETINIDE CTD 00007166	3.31E-07	$C_{26}H_{33}NO_2$	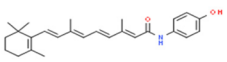
simvastatin CTD 00007319	3.31E-07	$C_{25}H_{38}O_5$	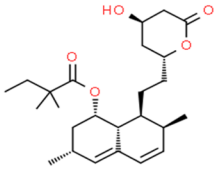
N-Acetyl-L-cysteine CTD 00005305	3.72E-07	$C_5H_9NO_3S$	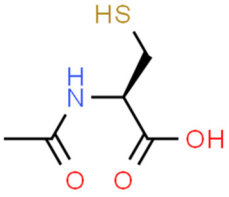
resveratrol CTD 00002483	4.78E-07	$C_{14}H_{12}O_3$	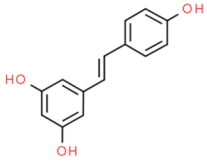
Sorafenib CTD 00004146	1.10E-06	$C_{21}H_{16}ClF_3N_4O_3$	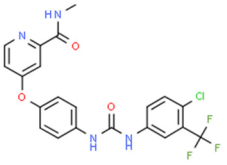

gender (Supplementary Table S4). qRT-PCR confirmed significant upregulation of both HSP90AA1 ($P<0.05$) and CAMP ($P<0.01$) in GBS patients compared to controls (Fig. 7C-D).

The consistent upregulation pattern was also observed in two independent public datasets. In the GSE211225 dataset, which includes whole blood mRNA samples from 6 acute-phase patients, 10 post-acute-phase patients, and 6 healthy controls, CAMP expression remained significantly elevated in the acute-phase patients compared to healthy controls ($P<0.05$)(Fig. 7E).Similarly, analysis of the GSE133750 dataset, derived from the sciatic nerves of Lewis rats with experimental autoimmune neuritis (EAN, an animal model that recapitulates key features of GBS), revealed significant upregulation of HSP90AA1 integrated the early neuritis, peak neuritis, and late neuritis stages compared to controls ($P<0.05$ (Fig. 7F).

This cross-species, cross-platform, and cross-tissue consistency robustly validates HSP90AA1 and CAMP as hub genes in the immunopathology of GBS.

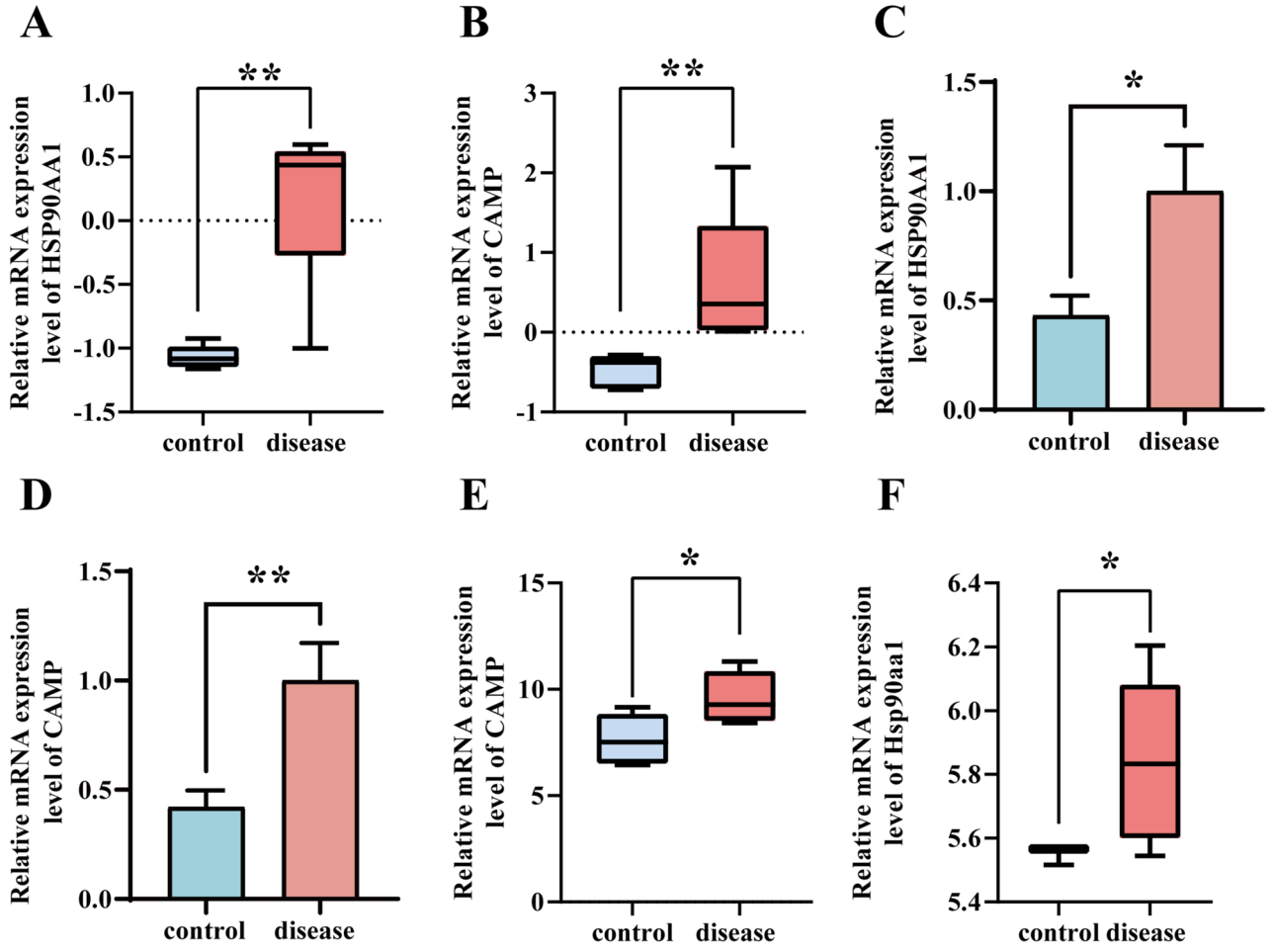

Fig. 7 Multi-level validation of hub gene upregulation in GBS. **A**-**B** Expression levels of HSP90AA1 (**A**) ($P < 0.01$) and CAMP (**B**) ($P < 0.01$) were significantly upregulated in peripheral blood leukocytes from GBS patients ($n = 7$) compared to healthy controls ($n = 5$) in the GSE31014 dataset.(C-D) qRT-PCR validation confirmed the significant upregulation of HSP90AA1 (**C**) ($P < 0.05$) and CAMP (**D**) ($P < 0.01$) in peripheral blood leukocytes from an independent cohort of acute-phase GBS patients ($n = 3$) compared to healthy controls ($n = 3$). **E** Validation in an independent human whole-blood mRNA dataset (GSE211225) confirmed significant upregulation of CAMP in acute-phase GBS patients ($n = 6$) compared to healthy controls ($n = 6$). ($P < 0.05$). **F** Cross-species validation in the sciatic nerves of Experimental Autoimmune Neuritis (EAN) rats (GSE133750 dataset) showed significant upregulation of Hsp90aa1 integrated all disease phases (early, peak, and late neuritis; $n = 9$) compared to healthy controls ($n = 3$). ($P < 0.05$)

Disscusion

This study employed an integrated approach that combined bioinformatics analysis with machine learning to delineate the key regulatory network within the peripheral immune microenvironment of GBS. Transcriptomic analysis confirmed immune activation and metabolic dysregulation within the peripheral immune compartment of GBS patients. Subsequently, a PPI network was constructed to identify a core gene module (Module I) and to extract a potentially functionally synergistic molecular unit from differentially expressed genes. Finally, two machine learning algorithms, LASSO and SVM-RFE, were applied for cross-validated screening. This process mitigated noise and multicollinearity in high-dimensional data and led to the precise identification of HSP90AA1 and CAMP as hub genes. Multifaceted approaches, including immune cell infiltration analysis, regulatory network construction, drug screening, and multidimensional validation, were utilized to investigate the functional mechanisms, upstream regulatory relationships, and potential therapeutic targets of the identified hub genes. These investigations provide new perspectives for elucidating the immunopathological mechanisms of GBS.

To transcend the limitations of a single-molecule/pathway perspective on a systems-level understanding of GBS, our study employed an integrated bioinformatics approach to map the coordinated dysregulation of immune and metabolic pathways. We systematically delineated this dysregulation at the transcriptomic level. GSEA revealed significant enrichment of key pathways in the GBS group, including chemokine signaling, Toll-like receptor signaling, B-cell receptor signaling, and oxidative phosphorylation. This is consistent with previous

literature, as infections such as Campylobacter jejuni can activate Toll-like and B-cell receptor signaling through molecular mimicry [2]. Furthermore, metabolic dysregulation, particularly the enhancement of oxidative phosphorylation, is essential for immune cell activation [36, 37]. Collectively, these pathways provide a macro-level perspective on immune hyperactivation and cellular energy metabolic imbalance, setting the stage for future mechanistic investigations.

To overcome the limitations of conventional differential expression analysis, which is confounded by gene collinearity and background noise and struggles to prioritize functionally central genes [16, 17], our study implemented a multi-step bioinformatics strategy. From PPI network to LASSO/SVM-RFE algorithms, we identify the most critical regulators within core gene module. This approach pinpointed HSP90AA1 and CAMP as key hub genes, a finding validated by their diagnostic potential in ROC curve analysis. This workflow mitigates the pitfalls of high-dimensional data analysis and surpasses traditional single-molecule approaches.

Our strategy also overcomes this limitation in immune microenvironment analysis, revealing the synergistic regulatory roles of these hub genes within the GBS immune network. In terms of adaptive immune regulation, HSP90AA1 exhibited significant immunostimulatory properties. Its expression was positively correlated with B cells and type 2 immune responses, and it was significantly enriched in both B-cell receptor and T-cell receptor signaling pathways, suggesting its involvement in GBS pathogenesis by promoting adaptive immune activation. This finding is consistent with existing research: as a key molecular chaperone, HSP90 maintains NF-κB pathway activation by stabilizing signaling molecules such as IKKβ, thereby promoting the release of pro-inflammatory factors such as TNF-α and IL-1β from microglia and exacerbating neuroinflammation [38, 39]. Furthermore, the regulatory role of HSP90 in the immune-neural axis further supports its central position in the GBS immune network [40, 41].In innate immunity and immune balance regulation, CAMP demonstrated a unique dual regulatory character. Its positive correlation with Tfh cells suggests a facilitative role in humoral immunity, while its negative correlation with activated $CD4^+$ T cells aligns with experimental findings that LL-37(the antimicrobial peptide encoded by CAMP) suppresses pathogenic $CD4^+$ T cells [42]. Notably, the significant negative correlation between CAMP and immunoregulatory CD56bright NK cells implies that it may disrupt immune homeostasis by impairing the IL-10-dependent immunosuppressive function of this subset [43]. This finding is consistent with studies showing that LL-37 promotes inflammatory responses in glial cells in neuroinflammation models [44, 45], collectively revealing the dual role of CAMP in GBS immune regulation, characterized by both "disinhibition" and "pro-inflammatory" effects.From a mechanistic perspective, the co-enrichment of HSP90AA1 and CAMP in the chemokine signaling pathway indicates that they may synergistically regulate immune cell migration and infiltration, jointly driving the progression of neuroinflammation in GBS.

To make the full multi-mechanism network, upstream key genes were identified. As a neuroinflammation suppressor, FOXC1 exerts anti-inflammatory and neuroprotective effects by inhibiting NLRP3 inflammasome activation and the NF-κB signaling pathway [46, 47]. This provides evidence that dysregulation of FOXC1 may be a critical upstream event driving the coordinated upregulation of HSP90AA1 and CAMP in GBS, initiating the immunoinflammatory cascade.

To expand translational potential, our study conducted a drug screening based on Core Module I. This approach identified eight candidate small molecules from the DSigDB database. Following a rigorous literature-based safety and mechanistic evaluation, five promising candidates were prioritized: Fenretinide, Simvastatin, N-acetylcysteine, Resveratrol, and Sorafenib, after excluding neurotoxicity or insufficient neurological evidences. Their mechanisms align with our core findings. Simvastatin and Sorafenib inhibit HSP90 chaperone function [32, 33]and Simvastatin also upregulates cAMP expression [35]and suppresses CCL2 [29], intersecting with the chemokine signaling pathway. The antioxidative and anti-inflammatory properties of N-acetylcysteine [31, 48–51], Fenretinide [52, 53], and Resveratrol [34, 54, 55]match the dysregulated oxidative phosphorylation and immune inflammatory signaling pathways. This "gene module–pathway–drug mechanism" convergence offers a rational and promising direction for GBS targeted therapy development.

This study employs an integrated bioinformatics approach to establish a framework that connects multi-hub gene expression with immune phenotypic dysregulation in GBS. Unlike traditional research that concentrates on individual molecules [40, 56–58], our machine-learning-based screening can simultaneously identify key hub genes, thus surpassing the "single-gene, single-function" paradigm. The application of ssGSEA was crucial in depicting the immune activation landscape, revealing coordinated upregulation in both adaptive and innate immune compartments. By correlating hub gene expression with the immune map, we identified distinct immunomodulatory patterns. ssGSEA provides a systems-level view of the immune microenvironment, extending beyond single-molecule studies and establishing a link between hub gene function and immune dysregulation in GBS.

Despite our integrative approach, this study has these limitations. First, the discovery and independent human validation cohorts were inherently limited by the rarity of GBS. Thus, future large-scale validation is essential but will require multicenter collaborations. Second, the ssGSEA-derived immune profile and predicted ceRNA network are computationally based and require experimental corroboration. Third, our functional associations remain correlative, and the causal roles of HSP90AA1 and CAMP must be tested through genetic interrogation in suitable models. Finally, the use of peripheral blood samples may not fully reflect the nerve microenvironment. Therefore, spatial transcriptomics of nerve tissues should be considered in future studies.

Looking forward, future research should focus on increasing the clinical sample size and directly confirming the roles of HSP90AA1 and CAMP in GBS experimental models via genetic manipulation techniques. Moreover, conducting systematic pharmacodynamic and mechanistic evaluations of the candidate small molecules identified in this study will greatly promote the development of targeted treatment strategies for GBS.

Conclusions

This study systematically delineates the immunopathological landscape of GBS through integrated bioinformatics and machine learning. We identified and validated HSP90AA1 and CAMP as key hub genes that coordinately induce immune inflammation dysregulation. Additionally, the identification of a common transcriptional regulator (FOXC1) and potential therapeutic compounds offers a translational roadmap. Despite its limitations, this work establishes HSP90AA1 and CAMP as central mediators and paves new avenues for targeted therapy in GBS.

Abbreviations

GBS	Guillain-Barré syndrome
GEO	Gene Expression Omnibus
GSEA	Gene Set Enrichment Analysis
ssGSEA	Single-Sample Gene Set Enrichment Analysis
DEGs	Differentially Expressed Genes
PPI	Protein-Protein Interaction
LASSO	Least Absolute Shrinkage and Selection Operator
SVM	Support Vector Machine
RFE	Recursive Feature Elimination
FDR	False discovery rate
PCA	Principal Component Analysis
NES	Normalized Enrichment Score
BCR	B-cell Receptor
HSPs	Heat Shock Proteins
RNA-seq	RNA sequencing
PPV	Positive predictive value
NPV	Negative predictive value
ceRNA	Competing endogenous RNA
NAC	N-acetylcysteine

Supplementary Information

The online version contains supplementary material available at https://doi.org/10.1186/s12883-026-04766-z.

Supplementary Material 1. Supplementary Figure 1. Sensitivity analysis confirms the robustness of Core Module I. The stability of the Core Module I was assessed by applying more stringent clustering parameters using the MCODE plugin. (A) Network identified with parameters set to Degree Cutoff = 3 and K-Core = 3. (B) Network identified with parameters set to Degree Cutoff = 4 and K-Core = 4

Supplementary Material 2. Supplementary Table 1. Primer sequences used for qRT-PCR validation

Supplementary Material 3. Supplementary Table 2. Diagnostic Performance of Hub Genes HSP90AA1 and CAMP

Supplementary Material 4. Supplementary Table 3. Comparison of Immune Cell Infiltration Levels between GBS Patients and Healthy Controls

Supplementary Material 5. Supplementary Table 4. Baseline characteristics of GBS patients and healthy controls in the qRT-PCR validation cohort

Acknowledgements

This study received assistance from the Science and Technology Research Center, Ningxia Medical University. We also thank the Neurology Center, General Hospital of Ningxia Medical University.

Authors' contributions

D.Z. and Z.W. conceptualized and designed the study. D.Z. performed bioinformatic analysis, analyzed the data, and wrote the original manuscript. Z.W. and W.M. collected the clinical samples. Z.W. reviewed and edited the first draft. All authors reviewed and approved the final manuscript.

Data availability

The data generated in this study will be available upon reasonable request. The R codes used for the differential expression analysis, feature selection are also available upon request. Interested researchers may direct their inquiries to the corresponding author.

Declarations

Ethics approval and consent to participate

This study was conducted in accordance with the principles of the Declaration of Helsinki. The study was conducted in accordance with the protocol approved by the Medical Research Ethics Review Committee of General Hospital of Ningxia Medical University (Ethics Number: 2018-318), and all examinations were carried out after obtaining written informed consent.

Consent for publication

Not applicable.

Competing interests

The authors declare no competing interests.

Author details

[1]Ning Xia Medical University, Yinchuan 750004, China
[2]Department of Geriatric Medicine, Shanxi Bethune Hospital, Shanxi Academy of Medical Science, Third Hospital of Shanxi Medical University, Tongji Shanxi Hospital, Taiyuan 030032, China
[3]General Hospital of Ningxia Medical University, Yinchuan 750004, China
[4]Institute of Medical Sciences, General Hospital of Ningxia Medical University, Yinchuan 750004, China
[5]Diagnosis and Treatment Engineering Technology Research Center of Nervous System Diseases of Ningxia, Yinchuan 750004, China
[6]Neurology Center, General Hospital of Ningxia Medical University, Yinchuan 750004, China

Received: 15 August 2025 / Accepted: 20 February 2026
Published online: 13 March 2026

References

1. Rajabally YA. Immunoglobulin and Monoclonal Antibody Therapies in Guillain-Barré Syndrome. Neurotherapeutics. 2022;19(3):885–96. https://doi.org/10.1007/s13311-022-01253-4.
2. Finsterer J. Triggers of Guillain-Barré Syndrome: Campylobacter jejuni Predominates. Int J Mol Sci. 2022;23(22). https://doi.org/10.3390/ijms232214222.
3. Zhang H, Zhao H, Yang G, Li Y, Liu Y. Gene Polymorphisms of Interleukin-27 Correlate with the Susceptibility, Severity, and Clinical Outcomes of Elderly People with Guillain-Barré Syndrome. Gerontology. 2022;68(8):854–60. https://doi.org/10.1159/000519227.
4. Khanmohammadi S, Malekpour M, Jabbari P, Rezaei N. Genetic basis of Guillain-Barre syndrome. J Neuroimmunol. 2021;358:577651. https://doi.org/10.1016/j.jneuroim.2021.577651.
5. Beydoun HA, Beydoun MA, Hossain S, Zonderman AB, Eid SM. Nationwide study of therapeutic plasma exchange vs intravenous immunoglobulin in Guillain-Barré syndrome. Muscle Nerve. 2020;61(5):608–15. https://doi.org/10.1002/mus.26831.
6. Petzold A, Hinds N, Murray NM, Hirsch NP, Grant D, Keir G, et al. CSF neurofilament levels: a potential prognostic marker in Guillain-Barré syndrome. Neurology. 2006;67(6):1071–3. https://doi.org/10.1212/01.wnl.0000237334.69665.92.
7. Matà S, Galli E, Amantini A, Pinto F, Sorbi S, Lolli F. Anti-ganglioside antibodies and elevated CSF IgG levels in Guillain-Barré syndrome. Eur J Neurol. 2006;13(2):153–60. https://doi.org/10.1111/j.1468-1331.2006.01161.x.
8. Isgrò MA, Bottoni P, Scatena R. Neuron-Specific Enolase as a Biomarker: Biochemical and Clinical Aspects. Adv Exp Med Biol. 2015;867:125–43. https://doi.org/10.1007/978-94-017-7215-0_9.
9. Berciano J. Axonal degeneration in Guillain-Barré syndrome: a reappraisal. J Neurol. 2021;268(10):3728–43. https://doi.org/10.1007/s00415-020-10034-y.
10. Li P, Wang S, Zhang R, Pei J, Chen L, Cao Y, et al. Identification of CSF biomarkers by proteomics in Guillain-Barré syndrome. Exp Ther Med. 2018;15(6):5177–82. https://doi.org/10.3892/etm.2018.6117.
11. Chiang HL, Lyu RK, Tseng MY, Chang KH, Chang HS, Hsu WC, et al. Analyses of transthyretin concentration in the cerebrospinal fluid of patients with Guillain-Barré syndrome and other neurological disorders. Clin Chim Acta. 2009;405(1–2):143–7. https://doi.org/10.1016/j.cca.2009.04.022.
12. Illes Z, Blaabjerg M. Cerebrospinal fluid findings in Guillain-Barré syndrome and chronic inflammatory demyelinating polyneuropathies. Handb Clin Neurol. 2017;146:125–38. https://doi.org/10.1016/b978-0-12-804279-3.00009-5.
13. Giesche N, Böhm-Gonzalez ST, Kleiser B, Kowarik MC, Dubois E, Stransky E, et al. Antiganglioside antibody frequency in routine clinical care settings. Eur J Neurol. 2024;31(7):e16290. https://doi.org/10.1111/ene.16290.
14. Naik GS, Meena AK, Reddy BAK, Mridula RK, Jabeen SA, Borgohain R. Anti-ganglioside antibodies profile in Guillain-Barré syndrome: Correlation with clinical features, electrophysiological pattern, and outcome. Neurol India. 2017;65(5):1001–5. https://doi.org/10.4103/neuroindia.NI_1226_15.
15. Kuwabara S, Kusunoki S, Kuwahara M, Yamano Y, Nishida Y, Ishida H, et al. Efficacy and safety of eculizumab in Guillain-Barré syndrome: A phase 3, multicenter, double-blind, randomized, placebo-controlled clinical trial. J Peripher Nerv Syst. 2024;29(3):339–49. https://doi.org/10.1111/jns.12646.
16. Subramaniam S, Hsiao G. Gene-expression measurement: variance-modeling considerations for robust data analysis. Nat Immunol. 2012;13(3):199–203. https://doi.org/10.1038/ni.2244.
17. Lawhorn CM, Schomaker R, Rowell JT, Rueppell O. Simple Comparative Analyses of Differentially Expressed Gene Lists May Overestimate Gene Overlap. J Comput Biol. 2018;25(6):606–12. https://doi.org/10.1089/cmb.2017.0262.
18. Chang KH, Chuang TJ, Lyu RK, Ro LS, Wu YR, Chang HS, et al. Identification of gene networks and pathways associated with Guillain-Barré syndrome. PLoS ONE. 2012;7(1):e29506. https://doi.org/10.1371/journal.pone.0029506.
19. Clark DJ, Dhanasekaran SM, Petralia F, Pan J, Song X, Hu Y, et al. Integrated Proteogenomic Characterization of Clear Cell Renal Cell Carcinoma. Cell. 2019;179(4):964–83. https://doi.org/10.1016/j.cell.2019.10.007.
20. Gao H, Wang S, Duan H, Wang Y, Zhu H. Biological analysis of the potential pathogenic mechanisms of Infectious COVID-19 and Guillain-Barré syndrome. Front Immunol. 2023;14:1290578. https://doi.org/10.3389/fimmu.2023.1290578.
21. Bindea G, Mlecnik B, Tosolini M, Kirilovsky A, Waldner M, Obenauf AC, et al. Spatiotemporal dynamics of intratumoral immune cells reveal the immune landscape in human cancer. Immunity. 2013;39(4):782–95. https://doi.org/10.1016/j.immuni.2013.10.003.
22. Xiang Z, Fang D, Gao D, Zhang Q, Zhang Y, Sun Y, et al. Interplay of axon regeneration genes and immune infiltration in spinal cord injury. J Transl Med. 2025;23(1):1034. https://doi.org/10.1186/s12967-025-06915-3.
23. Guo X, Hu W, Gao Z, Fan Y, Wu Q, Li W. Identification of PLOD3 and LRRN3 as potential biomarkers for Parkinson's disease based on integrative analysis. NPJ Parkinsons Dis. 2023;9(1):82. https://doi.org/10.1038/s41531-023-00527-8.
24. van Doorn PA, Van den Bergh PYK, Hadden RDM, Avau B, Vankrunkelsven P, Attarian S, et al. European Academy of Neurology/Peripheral Nerve Society Guideline on diagnosis and treatment of Guillain-Barré syndrome. J Peripher Nerv Syst. 2023;28(4):535–63. https://doi.org/10.1111/jns.12594.
25. Gaglio D, Bonanomi M, Valtorta S, Bharat R, Ripamonti M, Conte F, et al. Disruption of redox homeostasis for combinatorial drug efficacy in K-Ras tumors as revealed by metabolic connectivity profiling. Cancer Metab. 2020;8:22. https://doi.org/10.1186/s40170-020-00227-4.
26. Nooh M, Hakemi-Vala M, Nowroozi J, Fatemi SR, Dezfulian M. Prediction of Blood miRNA-mRNA Regulatory Network in Gastric Cancer. Rep Biochem Mol Biol. 2021;10(2):243–56. https://doi.org/10.52547/rbmb.10.2.243.
27. Li Z, Huang F, Hao S. Guillain-Barré syndrome in patients with multiple myeloma: three cases report and literature review. BMC Neurol. 2025;25(1):36. https://doi.org/10.1186/s12883-025-04045-3.
28. Ceolin V, Cenna R, Resente F, Spadea M, Fagioli F, Bertorello N. Guillain-Barré syndrome after bortezomib therapy in a child with relapsed acute lymphoblastic leukemia. Pediatr Hematol Oncol. 2022;39(2):187–92. https://doi.org/10.1080/08880018.2021.1959691.
29. Langert KA, Von Zee CL, Stubbs EB Jr. Cdc42 GTPases facilitate TNF-α-mediated secretion of CCL2 from peripheral nerve microvascular endoneurial endothelial cells. J Peripher Nerv Syst. 2013;18(3):199–208. https://doi.org/10.1111/jns5.12032.
30. Zhang X, Jin J, Peng X, Ramgolam VS, Markovic-Plese S. Simvastatin inhibits IL-17 secretion by targeting multiple IL-17-regulatory cytokines and by inhibiting the expression of IL-17 transcription factor RORC in CD4 + lymphocytes. J Immunol. 2008;180(10):6988–96. https://doi.org/10.4049/jimmunol.180.10.6988.
31. Singh M, Kim A, Young A, Nguyen D, Monroe CL, Ding T, et al. The Mechanism and Inflammatory Markers Involved in the Potential Use of N-acetylcysteine in Chronic Pain Management. Life (Basel). 2024;14(11). https://doi.org/10.3390/life14111361.
32. Kou X, Jiang X, Liu H, Wang X, Sun F, Han J, et al. Simvastatin functions as a heat shock protein 90 inhibitor against triple-negative breast cancer. Cancer Sci. 2018;109(10):3272–84. https://doi.org/10.1111/cas.13748.
33. Booth L, Roberts JL, Tavallai M, Chuckalovcak J, Stringer DK, Koromilas AE, et al. [Pemetrexed + Sorafenib] lethality is increased by inhibition of ERBB1/2/3-PI3K-NFκB compensatory survival signaling. Oncotarget. 2016;7(17):23608–32. https://doi.org/10.18632/oncotarget.8281.
34. Wang SJ, Bo QY, Zhao XH, Yang X, Chi ZF, Liu XW. Resveratrol pre-treatment reduces early inflammatory responses induced by status epilepticus via mTOR signaling. Brain Res. 2013;1492:122–9. https://doi.org/10.1016/j.brainres.2012.11.027.
35. Lüthje P, Walker S, Kamolvit W, Mohanty S, Pütsep K, Brauner A. Statins influence epithelial expression of the anti-microbial peptide LL-37/hCAP-18 independently of the mevalonate pathway. Clin Exp Immunol. 2019;195(2):265–76. https://doi.org/10.1111/cei.13217.
36. Iwasaki Y, Takeshima Y, Fujio K. Basic mechanism of immune system activation by mitochondria. Immunol Med. 2020;43(4):142–7. https://doi.org/10.1080/25785826.2020.1756609.
37. Barfüßer C, Wiedemann C, Hoffmann ALC, Hirmer S, Deeg CA. Altered Metabolic Phenotype of Immune Cells in a Spontaneous Autoimmune Uveitis Model. Front Immunol. 2021;12:601619. https://doi.org/10.3389/fimmu.2021.601619.
38. Cheng J, Wu L, Chen X, Li S, Xu Z, Sun R, et al. Polo-like kinase 2 promotes microglial activation via regulation of the HSP90α/IKKβ pathway. Cell Rep. 2024;43(10):114827. https://doi.org/10.1016/j.celrep.2024.114827.
39. Guo J, Li CG, Mai FY, Liang JR, Chen ZH, Luo J, et al. Lithospermic acid targeting heat shock protein 90 attenuates LPS-induced inflammatory response via NF-κB signalling pathway in BV2 microglial cells. Immunol Res. 2025;73(1):54. https://doi.org/10.1007/s12026-025-09600-1.
40. Beretta G, Shala AL. Impact of Heat Shock Proteins in Neurodegeneration: Possible Therapeutical Targets. Ann Neurosci. 2022;29(1):71–82. https://doi.org/10.1177/09727531211070528.
41. Fan X, Sun L, Qin Y, Liu Y, Wu S, Du L. The Role of HSP90 Molecular Chaperones in Depression: Potential Mechanisms. Mol Neurobiol. 2025;62(1):708–17. https://doi.org/10.1007/s12035-024-04284-4.

42. Veremeyko T, Yung AWY, Dukhinova M, Kuznetsova IS, Pomytkin I, Lyundup A, et al. Cyclic AMP Pathway Suppress Autoimmune Neuroinflammation by Inhibiting Functions of Encephalitogenic CD4 T Cells and Enhancing M2 Macrophage Polarization at the Site of Inflammation. Front Immunol. 2018;9:50. https://doi.org/10.3389/fimmu.2018.00050.
43. Poli A, Michel T, Thérésine M, Andrès E, Hentges F, Zimmer J. CD56bright natural killer (NK) cells: an important NK cell subset. Immunology. 2009;126(4):458–65. https://doi.org/10.1111/j.1365-2567.2008.03027.x.
44. Bhusal A, Nam Y, Seo D, Rahman MH, Hwang EM, Kim SC, et al. Cathelicidin-related antimicrobial peptide promotes neuroinflammation through astrocyte-microglia communication in experimental autoimmune encephalomyelitis. Glia. 2022;70(10):1902–26. https://doi.org/10.1002/glia.24227.
45. Lee M, Shi X, Barron AE, McGeer E, McGeer PL. Human antimicrobial peptide LL-37 induces glial-mediated neuroinflammation. Biochem Pharmacol. 2015;94(2):130–41. https://doi.org/10.1016/j.bcp.2015.02.003.
46. Wang H, Wang H, Song Y, Liu C, Qian X, Zhang D, et al. Overexpression of Foxc1 ameliorates sepsis–associated encephalopathy by inhibiting microglial migration and neuroinflammation through the IκBα/NF–κB pathway. Mol Med Rep. 2022;25(3). https://doi.org/10.3892/mmr.2022.12623.
47. Yang P, Yu Q. Downregulation of FOXC1 Modified by METTL3/YTHDF1 Axis Aggravates NLRP3-Mediated Inflammasomes Formation and Cell Pyroptosis in Epilepsy. Faseb j. 2025;39(17):e70987. https://doi.org/10.1096/fj.202500188R.
48. Victor VM, Rocha M, De la Fuente M. N-acetylcysteine protects mice from lethal endotoxemia by regulating the redox state of immune cells. Free Radic Res. 2003;37(9):919–29. https://doi.org/10.1080/1071576031000148727.
49. Sakai M, Yu Z, Taniguchi M, Picotin R, Oyama N, Stellwagen D, et al. N-Acetylcysteine Suppresses Microglial Inflammation and Induces Mortality Dose-Dependently via Tumor Necrosis Factor-α Signaling. Int J Mol Sci. 2023;24(4). https://doi.org/10.3390/ijms24043798.
50. Park S, Park JA, Yoo H, Park HB, Lee Y. Proteasome inhibitor-induced cleavage of HSP90 is mediated by ROS generation and caspase 10-activation in human leukemic cells. Redox Biol. 2017;13:470–6. https://doi.org/10.1016/j.redox.2017.07.010.
51. Licks F, Minuzzo Hartmann R, Schemitt E, Raskopf Colares J, Marques C, Fillmann H, et al. Synergistic antioxidant and anti-inflammatory action of N-acetylcysteine in portal hypertensive gastropathy in rats. Hepatol Forum. 2022;3(2):51–6. https://doi.org/10.14744/hf.2021.2021.0034.
52. Li T, Zheng LN, Han XH. Fenretinide attenuates lipopolysaccharide (LPS)-induced blood-brain barrier (BBB) and depressive-like behavior in mice by targeting Nrf-2 signaling. Biomed Pharmacother. 2020;125:109680. https://doi.org/10.1016/j.biopha.2019.109680.
53. Potenza RL, Lodeserto P, Orienti I. Fenretinide in Cancer and Neurological Disease: A Two-Face Janus Molecule. Int J Mol Sci. 2022;23(13). https://doi.org/10.3390/ijms23137426.
54. Zhang F, Wang H, Wu Q, Lu Y, Nie J, Xie X, et al. Resveratrol protects cortical neurons against microglia-mediated neuroinflammation. Phytother Res. 2013;27(3):344–9. https://doi.org/10.1002/ptr.4734.
55. Ma S, Fan L, Li J, Zhang B, Yan Z. Resveratrol promoted the M2 polarization of microglia and reduced neuroinflammation after cerebral ischemia by inhibiting miR-155. Int J Neurosci. 2020;130(8):817–25. https://doi.org/10.1080/00207454.2019.1707817.
56. Zhao A, Zhang G, Wei H, Yan X, Gan J, Jiang X. Heat shock proteins in cerebral ischemia-reperfusion injury: Mechanisms and therapeutic implications. Exp Neurol. 2025;390:115284. https://doi.org/10.1016/j.expneurol.2025.115284.
57. Xin M, Feng J, Hao Y, You J, Wang X, Yin X, et al. Cyclic adenosine monophosphate in acute ischemic stroke: some to update, more to explore. J Neurol Sci. 2020;413:116775. https://doi.org/10.1016/j.jns.2020.116775.
58. Guijarro-Belmar A, Domanski DM, Bo X, Shewan D, Huang W. The therapeutic potential of targeting exchange protein directly activated by cyclic adenosine 3',5'-monophosphate (Epac) for central nervous system trauma. Neural Regen Res. 2021;16(3):460–9. https://doi.org/10.4103/1673-5374.293256.

Publisher's note